Carbon segregation in screw dislocation in BCC tungsten: when two phase transitions intertwine

Fabienne Berthier, Bernard Legrand

Carbon segregation in screw dislocation in BCC tungsten: when two phase transitions intertwine.

F. Berthier[1*], B. Legrand[2]

[1]Université Paris-Saclay, CNRS, Institut de chimie moléculaire et des matériaux d'Orsay, 91405 Orsay, France

[2]Université Paris-Saclay, CEA, Service de Métallurgie Physique, 91191 Gif-sur-Yvette, France

*fabienne.berthier@universite-paris-saclay.fr

Key words

Segregation, phase transition, order, phase separation, carbon, tungsten, dislocation

Abstract

Recently some authors have investigated the segregation of carbon in screw dislocations of tungsten [1]. They show that screw dislocations remain fully saturated by carbon atoms and then they studied the mobility of the saturated dislocation [2]. However, their model assumes that all octahedral lines of the dislocation have identical behavior. One can wonder whether by releasing this constraint ordering phenomena could occur. In this paper, we study the segregation of carbon on the different sites of the dislocation using a Mean-Field model and Monte Carlo simulations based on the same interaction energies between carbon and screw dislocations in tungsten as in [1]. One obtains a very different behavior from that observed in the original paper, due to a strong repulsive inter-line interaction.

1. Introduction

Plasticity is mainly driven by the glide of dislocations. In the case of alloys, the local chemical composition on dislocation sites differs from bulk, which can modify their mobility relative to the pure metal. It is therefore essential to understand the chemical effects on dislocations.

More generally, previous works have shown the importance of segregation on the physical and chemical properties of polycrystalline materials. Segregation is a very well documented phenomenon, both from the experimental and from the theoretical point of view. At the atomic scale, it has already been possible to characterize surface segregation with STM [3,4], grain boundaries and dislocation segregation by HREM [5], ToF-FIM [6] and with the three-dimensional atomic probe (ATP) [7–9] which can lead to atomic resolution. Theoretically segregation at interfaces has also motivated intensive research at surfaces [10–13], grain-boundaries [14–17], dislocations [18,19], nanoparticles [20–24] and nanowires [25].

Recently some authors have studied the segregation of carbon atoms on a tungsten screw dislocation [1]. They have shown that the presence of interstitial carbon atoms induces a reconstruction of the $1/2\ \langle 111 \rangle$ screw dislocation core from its so-called easy core configuration to a hard-core configuration, along with an attractive interaction energy. The carbon atom is located at the centre of a regular trigonal prism. Ab initio calculations show that carbon segregation is favored on prismatic P sites and on octahedral $O^{(4)}$ sites. However, in absolute value, the segregation energy is larger for the prismatic sites (-2.1 eV instead of -1.5 eV). The intra-line interaction energies, *i.e*. between two carbon atoms belonging to the same line (prismatic or octahedral), are attractive, whereas the inter-line interaction energies between $P - O^{(4)}$ and $O^{(4)} - O^{(4)}$ are repulsive. Thus, the

ground state maybe complex and one can expect an inter-line ordering. The authors have developed a Mean Field model (MF) to determine the carbon concentration on the dislocation lines P and $O^{(4)}$ as a function of temperature by assuming that all octahedral lines have the same composition.

The original article [1] asks to answer the following questions :

(1) Could ordering phenomena occur at the core of dislocations? It is well known that for a one-dimensional system the answer is no, but the dislocation is not really a one-dimensional system. Order-disorder or demixtion-disorder transitions are therefore possible and can be observed even in Monte Carlo (MC). One can wonder if such transitions exist in this case.

(2) What is the physical origin of the value of the $O^{(4)}$ line concentration ($c_{O^{(4)}} \approx 0.9$), which differs from 0 or 1 at low temperature? The authors argue that repulsive interactions are the cause. Is a link with ordering phenomena possible?

(3) What is the influence of density of dislocations on the different sites of the core dislocation as a function of the temperature and of the bulk concentration?

So, the aim of the present article is to investigate the segregation of carbon in screw dislocations in tungsten using a model that allows the observation of possible intra- and inter-line transitions.

The paper is organized as follows. After the description of the energetic model in section 2, we present the computational methods (section 3), including in particular the description of the mean-field model which differs from the original paper. Section 4 details results obtained with mean-field modelling. Section 4.3 compares these results with the Monte Carlo results. Finally, we discuss the main features of the thermodynamics of the considered system (section 5).

2. Energetic parameters

We consider the energetic model of the original work [1] which was determined from *ab initio* calculations. The energy of the reconstructed dislocation is given by an Ising Hamiltonian:

$$H = H_0 + \sum_i \Delta E_i^{seg,0} \sigma_i + \sum_{i,j \neq i} V_{ij} \sigma_i \sigma_j. \quad (1)$$

The Hamiltonian depends on two elements, the segregation energies $\Delta E_i^{seg,0}$ in dilute limit on site i and the pair interaction energies V_{ij} between carbon atoms on two sites i and j. Both the prismatic P sites inside the dislocation core and the six different $O^{(4)}$ sites around the reconstructed core are taken into account (see *figure 1a*). In the following, in order to simplify the notations, the octahedral lines $O^{(4)}$ are named O. H_0 is a constant term, proportional to the energetic cost to transform a dislocation segment from an easy to a hard core. σ_i is an occupation number, which equals 1 if the site i is occupied by an atom, and 0 otherwise. The interactions between atoms are restricted to the nearest neighbor sites.

The segregation energy is the energy variation in dilute limit between an initial configuration and a final configuration where a carbon atom is respectively located in a site of the bulk and in a site on the dislocation. The segregation energies on sites P (in the hard configuration induced to the carbon segregation) and on sites O are respectively equals to $\Delta E_P^{seg,0} = -2.1$ eV and $\Delta E_O^{seg,0} = -1.38$ eV. The segregation energy is twice higher (in absolute value) on P sites than on O sites. That means that carbon segregation is strongly favored in the P line.

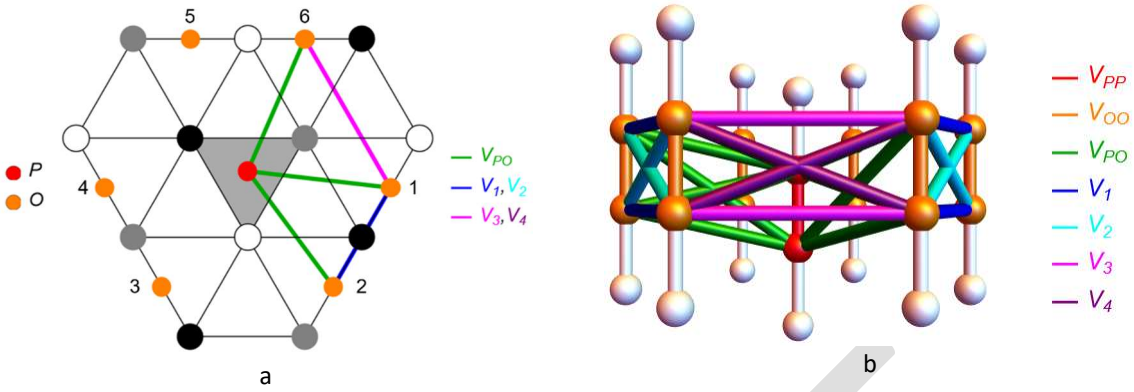

Fig. 1: *(a) Projection on the (111) plane of the tungsten (in white, black and grey) and carbon (in color) atomic positions around the reconstructed dislocation core (represented by a grey triangle). The prismatic site P inside the hard core is represented with a red disk while the O_k sites, with k ranging from 1 to 6, are represented by orange disks. Schematic representation of the alloying pair interactions between P and O sites: (a) in projection along the Burgers vector direction and (b) in perspective perpendicular to the Burgers vector. The interaction terms V_{PP}, V_{PO}, V_{OO}, V_1, V_2, V_3 and V_4 are represented in red, dark green, orange, blue, cyan, magenta and purple, respectively.*

The interaction energies between two carbon atoms belonging to the same line P and O are $V_{PP} = -0.08$ eV and $V_{OO} = -0.27$ eV (see *figure 1b*). These interactions are attractive. The system tends to form homoatomic intra-line bonds. The interaction intra-line on the P line is weak (almost nil) and strong on the O line. Intra-line phase separation can therefore be expected on line P and especially on line O.

All the inter-line interactions are repulsive: $V_{PO} = 0.06$ eV, $V_1 = 0.25$ eV, $V_2 = 0.61$ eV, $V_3 = 0.18$ eV and $V_4 = 0.13$ eV (see *figure 1a and 1b*). The tendency to form heteroatomic bonds between the P line and O lines is weak and strong between two neighboring O lines. Therefore, the possibility of observing ordered inter-O-line structures cannot be excluded.

3. Computational Methods

Based on the attractive intra-line and repulsive inter-line interaction energies, the system may present ordered structures and simulations have to allow this complexity.

3.1 Monte Carlo simulations

We perform Metropolis Monte Carlo simulations in the grand canonical ensemble, which enables the optimization of both the number and distribution of the carbon atoms on the different sites. Only one type of event is included. Incorporation and extraction of carbon atoms are proposed. A site is chosen randomly. If the site is empty then the incorporation of a carbon atom is proposed, otherwise extraction is proposed. A trial is accepted/rejected following the Metropolis algorithm [26]. The probabilities of incorporation and extraction are respectively:

$$P_I = \frac{N}{N_C+1}\exp\left(-\frac{\Delta E_I-\mu}{k_BT}\right) \text{ and } P_E = \frac{N_C}{N}\exp\left(-\frac{\Delta E_E-\mu}{k_BT}\right) \quad (2)$$

with N the number of sites and N_C the number of carbon atoms in the cell. ΔE_I (respectively ΔE_E) represents the energy variation due to the incorporation (resp. extraction) of a carbon atom. Each energy is given by the Hamiltonian (eq. 1) which depends on the configuration via the site occupation numbers. μ is the chemical potential which is calculated from the mean-field formalism in dilute limit:

$$\mu = E_0 + k_B T \ln \frac{c_{bulk}}{1-c_{bulk}} \quad (3)$$

where E_0 is the incorporation energy of one isolated carbon atom into a bulk octahedral site and c_{bulk} the concentration of carbon. Interaction between carbon atoms in the bulk are neglected which is available for bulk concentrations lower than 1000 appm as considered here. The bulk solubility limit should also be considered especially when $T \to 0$ K. According to the experimental phase diagram, the solubility limit is less than 0.3 % (3000 appm) [27].

Monte Carlo simulations allow the determination of isotherms and isoconcentrations, *i.e.* the evolution of the concentration of the dislocation sites as a function of the chemical potential (or as a function of the bulk concentration) at a given temperature and respectively as a function of temperature for a fixed value of the bulk concentration.

The simulation box contains the line of prismatic P sites and the six lines of octahedral O sites. Each line is composed of $l_d = 100$ sites. The total number of sites is $N = 700$ and the number of MC macro steps is $N_{MC} = 10^6$. Periodic boundary conditions are used. Hereafter we will not present the concentrations per site but the concentrations of lines $c_X = \frac{1}{N_{MC}} \sum_{N_{MC}} \frac{1}{l_d} \sum_{n=1}^{l_d} \sigma_n$, with σ_n the occupation number and $X = P$ or O_i, with $i = 1, \dots, 6$.

In addition, we calculate the Warren-Cowley short-range order parameter (SRO):

$$\alpha_{XY} = 1 - l_d \frac{N_{C_X E_Y}}{Z_{XY} N_{C_X} (l_d - N_{C_X})} \quad (4)$$

with $X, Y = P$ or O_i, $i = 1, \dots, 6$; $N_{C_X E_Y}$ the number of first neighboring pairs with a carbon atom (C) on line X and an empty site (E) on line Y; N_{C_X} the number of carbon atom (C) on line X and Z_{XY} the inter-line $X - Y$ coordination number.

3.2 Mean-Field modelling

We also perform mean-field calculations which allow a detailed analysis of results. The great advantage of MF modeling is to explore exhaustively all the concentration profiles that are solutions of the system. Given the repulsive interactions between the O lines and thus the possibility that the system forms an ordered inter-O-line structure we have considered the P line and two O lines (lines 1 and 2 for example, see *figure 1a*). We have verified that the results are identical to those of a more complete model including the P-line and the six O lines or even the with per-site formalism.

Using the Bragg-Williams approximation, the minimization of the free energy leads to the well-known segregation equation:

$$\frac{c_X}{1-c_X} = \frac{c_{bulk}}{1-c_{bulk}} exp\left(-\frac{\Delta E_X^{seg}}{k_B T}\right), \quad (5)$$

With $X = 0, 1, 2$ respectively for the P, O_1 and O_2 lines. ΔE_X^{seg} the segregation energy in the X line:

$$\begin{cases} \Delta E_P^{seg} = \Delta E_P^{seg,0} + 2\,V_{PP} c_0 + 6\,V_{PO}(c_1 + c_2) \\ \Delta E_{O_1}^{seg} = \Delta E_O^{seg,0} + 2\,V_{PO} c_0 + 2\,V_{OO} c_1 + (V_1 + 2V_2 + V_3 + 2V_4) c_2 \\ \Delta E_{O_2}^{seg} = \Delta E_O^{seg,0} + 2\,V_{PO} c_0 + 2\,V_{OO} c_2 + (V_1 + 2V_2 + V_3 + 2V_4) c_1 \end{cases} \quad (6)$$

The total inter-O-line interaction energy $V_1 + 2V_2 + V_3 + 2V_4 = 1.91$ eV is very high, which strengthens the assumption of an inter-O-line ordering. Such order is characterized by the long-range order parameter (LRO) $\eta = c_1 - c_2$, which implies describing the two O-lines separately. A mean-field model

with a single O-line, *i.e.* that assumes a homogeneous distribution on all O-lines, cannot account for an inter O-line order.

Solving equation 5 gives the carbon concentration on the different lines for an isolated dislocation. To take into account the dislocation density ρ, we consider the conservation of matter that relates the bulk carbon concentration to the nominal concentration as following $\frac{N_{bulk}}{3} c_{nom} = N_{bulk} c_{bulk} + N_P c_P + N_O \sum_i c_{O_i}$ with $N_{bulk} = \frac{6V}{a^3}$, $N_P = \frac{\rho V}{b}$ and $N_O = N_P$ for a volume V with a lattice parameter a and the dislocation burgers vector b. After simplification, with the notations defined above, this relationship becomes:

$$c_{nom} = 3c_{bulk} + 3\rho \frac{a^3}{6b}\left(c_0 + 3\,(c_1 + c_2)\right). \quad (7)$$

4. Results

If Monte Carlo simulations are a very efficient method to characterize the segregation phenomena, the SRO and LRO, it is only a numerical method. The mean-field modelling has the advantage to be analytical, which permits an easy analysis of the thermodynamic driving forces. Moreover, we can quickly test the whole range of temperature and concentration. Therefore, we first present the mean-field results, and complete the study by comparison with Monte Carlo.

4.1 Isotherms

In Figure 2, the segregation isotherms are shown at $T = 2000$ K, giving the concentration of the three lines $P, O_1, O_2 : c_0$, c_1 and c_2, as a function of the bulk concentration c_{bulk}. As the segregation energy on the P line is higher (in absolute value) than that on the O lines, the enrichment is more important on the P line whatever c_{bulk}. As suspected, due to the strong repulsive interaction between the O lines, the O lines split into two groups (within a range of temperature and concentration): rich and poor lines. The separation of one isotherm in two isotherms is the signature of an order-disorder transition.

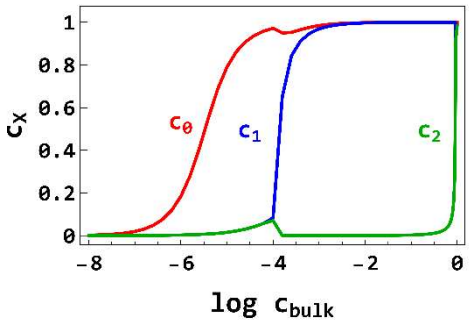

Fig. 2: Equilibrium segregation isotherms for the prismatic P line (in red) and for the octahedral O_1 (in blue) and O_2 (in green) lines of the screw dislocation at $T = 2000\ K$.

To obtain the phase diagram associated to this transition, we calculate the isotherms at various temperatures. *Figure 3a* shows the isotherms as a higher temperature ($T = 5000$ K). As the temperature is increased (but still below the order-disorder temperature), the isotherms on the different lines are shifted to higher bulk concentrations, the slope of the isotherms and the enrichment factor c_X/c_{bulk} decrease. The transition that is characterized by the separation of the O lines into two groups is bounded at a given temperature in a bulk concentration range $c_{bulk} \in [c_{b1}, c_{b2}]$ and in an O line concentration range by the solubility limits c_α and c_β (see *figure 3a*). Note that in this domain, the average O isotherm $\langle c_O \rangle$ is a monotonic increasing function.

As the temperature increases, these limits decrease (see *figure 3b and 3c*). *Figure 3b* displays the diagram of existence of order (c_{bulk}, T). The diagram is asymmetric, the limit c_{b1} varies little while c_{b2} varies a lot with temperature. For a bulk concentration c_{bulk} between c_{b1} and c_{b2} the structure is ordered with a carbon-rich O_1 line and a carbon-poor O_2 line whose respective concentrations are given by the isotherms for the c_{bulk} value. The phase diagram of O-lines $(\langle c_O \rangle, T)$ is more symmetric (*figure 3c*). For an average concentration $\langle c_O \rangle$ of the O lines between c_α and c_β the composition of each line is given by the isotherms at the horizontal of $\langle c_O \rangle$.

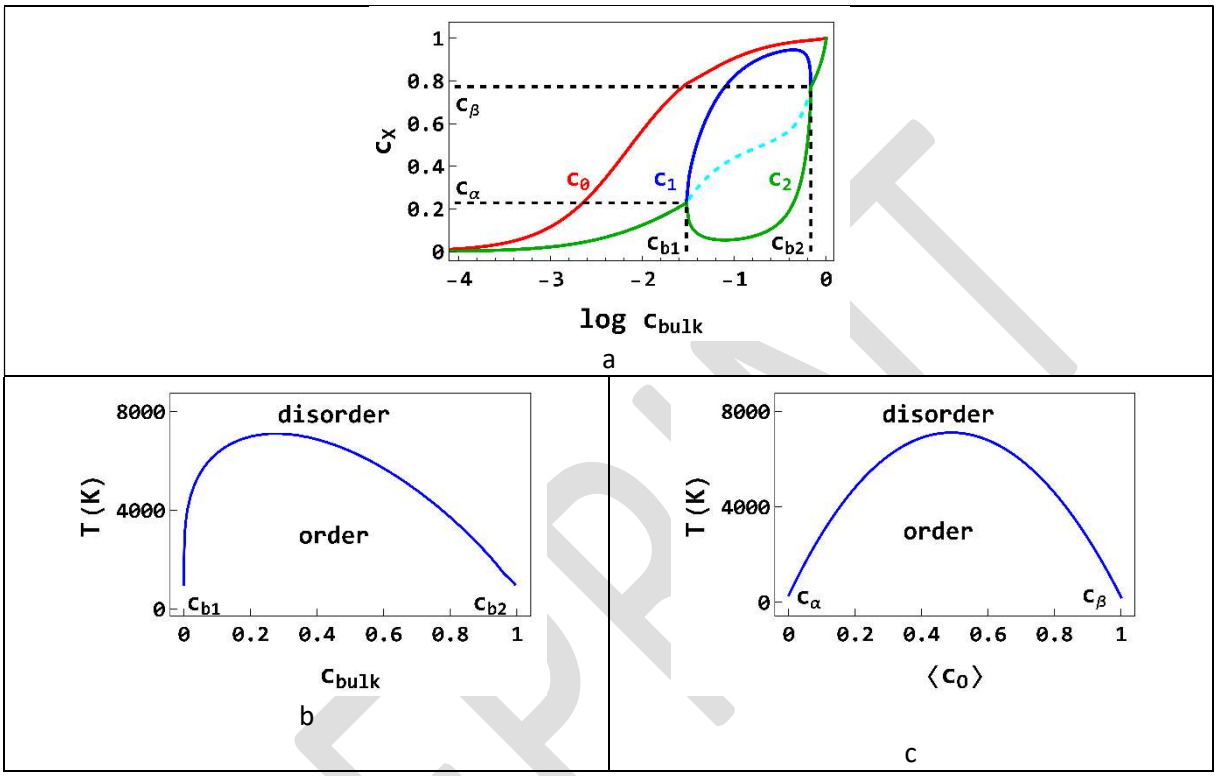

Fig. 3: Equilibrium segregation isotherms for the prismatic P line (in red) and for the octahedral O_1 (in blue), O_2 (in green) lines and for the average isotherm of O lines (in cyan) of the screw dislocation at $T = 5000\ K$ (a), domain of existence of the ordered states in c_{bulk} (b), phase diagram of ordered state in $\langle c_O \rangle$ (c).

As the temperature decreases, the isotherm c_1 of the rich O line presents a van der Waals loop, indicating an intra-line transition of first order (see *figure 4a*). This demixtion/disorder transition is due to the attractive interaction between carbon-carbon atoms on the same O line. We can use the rule of equal areas to obtain the solubility limits. This rule ensures that the two phases, one rich and the other one poor in carbon, have the same free energy. The isotherm of line P shows the same behavior at even lower temperatures. The intra-O critical temperature T_c^O, below which a first order phase transition is observed on the O line, is slightly less than 1600 K. The same consideration for the c_0 curve leads to an estimation of T_c^P about 500 K. The demixtion/disorder critical temperature for the O lines is higher than that for the P line. The intra-line phase diagrams, obtained by drawing the solubility limits, present a miscibility gap (see *figure 4b*).

The intra-line critical temperatures given by $T_c^X = -\frac{Z\,V_{XX}}{4\,k_B}$ in the mean-field approximation are overestimated compared to the exact calculation obtained in Monte Carlo. For a one-dimensional system, the critical temperature is expected to be 0 in the Monte Carlo method. The signature of the phase transition should be characterized by a strong local homoatomic order along these lines.

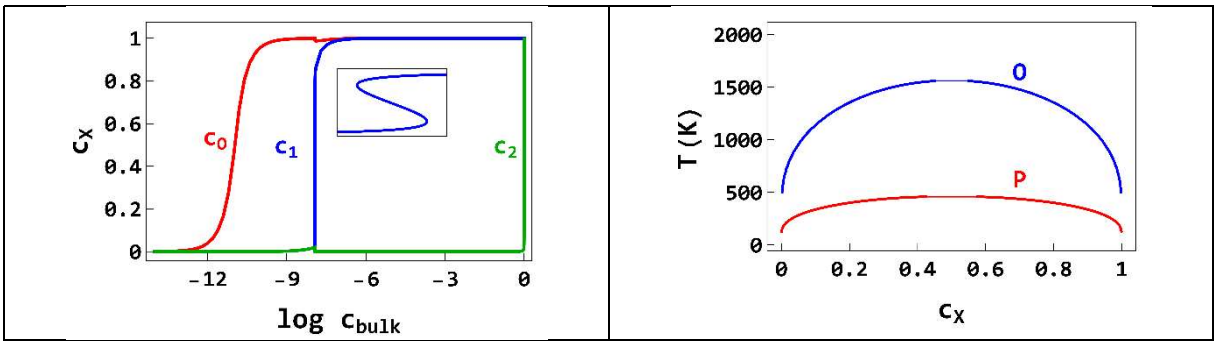

Fig. 4: Equilibrium segregation isotherms for the prismatic P line (in red) and for the octahedral O_1 (in blue) and O_2 (in green) lines of the screw dislocation at $T = 1000\ K$ (a) and intra-lines phase diagram P and O (b).

To summarize the main thermodynamic properties of the three lines model, note that

- there are two transitions which affect the lines O: one order-disorder (related to the repulsive interactions between lines O), the other demixtion-disorder (related to the attractive intra-line interactions O) with thus a phase diagram (in c_{bulk} and T (*figure 3b*) or, easier to draw, in c_O and T (*figure 4c*)). These transitions have almost no effect on the P line.
- there is a demixtion-disorder transition affecting the P-line related to the weak attractive interactions V_{PP} on the P-line leading to a critical mean field temperature close to 500 K. Phase separation on the P-line occurs at low temperatures and at very low bulk concentration (of about 10^{-2}).

4.2 Isoconcentrations

The evolution of the concentration profile as a function of temperature is shown in *figure 5a* for c_{nom} equal to 10 and 100 appm. The P line is fully saturated in carbon atoms at low temperatures up to about 2000 K for these nominal concentrations. Then when the temperature increases the concentration decreases. For O lines, without the constraint that all the lines O have identical behavior, we obtain a behavior very different from the one observed with this constraint (as in the original paper). The strong repulsive inter-O-lines interaction leads to an order-disorder transition at low temperatures which is characterized by a separation in two groups of the O lines, one rich and the other poor in carbon. This yields more classical result with line concentrations equal to 1 or 0 when $T \to 0$ K (*figure 5a*).

The temperature T_m^X at which the concentration of the line X is equal to $c_X = 0.5$ can easily be calculated by assuming that the lines are independent. The system is thus reduced to a single equation that describes the evolution of c_X with temperature $\frac{c_X}{1-c_X} = \frac{c_{bulk}}{1-c_{bulk}} exp\left(-\frac{\Delta E_X^{seg}}{k_B T}\right)$ and $c_{bulk} = c_{nom}/3$. To obtain the expression of T_m^X additional assumptions are required:

- $c_1 = c_2 = 0$ for the P line. We then obtain the following expression $T_m^P = \left(\Delta E_P^{seg,0} + V_{PP}\right) / k_B \ln \frac{c_{bulk}}{1-c_{bulk}}$. This formula leads to $T_m^P = 2451$ K for $c_{nom} = 100$ appm and $T_m^P = 2003$ K for $c_{nom} = 10$ appm.
- $c_0 = 1$ and $c_2 = 0$ for the O line rich in carbon O_1. T_m^O is then given by $T_m^O = \left(\Delta E_O^{seg,0} + 2\,V_{PO} + V_{OO}\right) / k_B ln \frac{c_{bulk}}{1-c_{bulk}}$ which yields $T_m^O = 1720$ K for $c_{nom} = 100$ appm and $T_m^O = 1406$ K for $c_{nom} = 10$ appm.

This simplified model gives values in perfect agreement with full calculations (*figure 5a*).

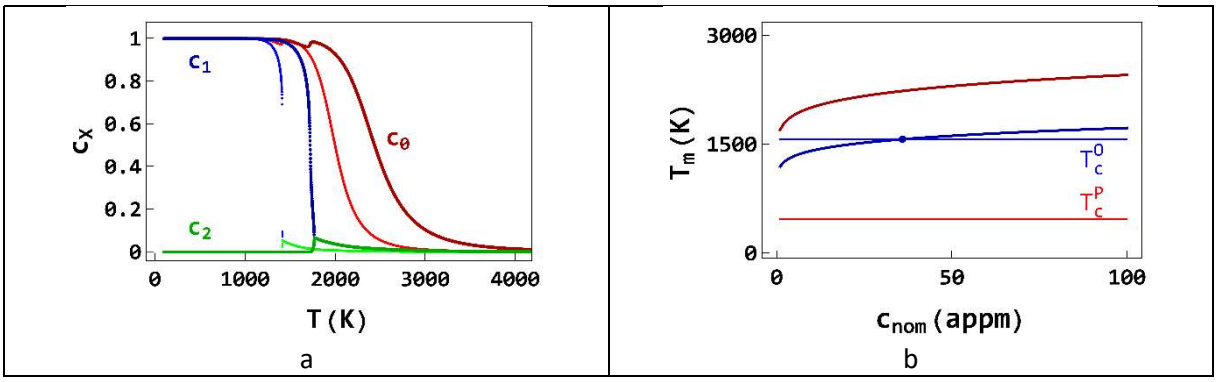

Fig. 5: Evolution of c_0 (in red), c_1 (in blue) and c_2 (in green) concentrations with respect to the temperature for $c_{nom} = 10$ (light) and 100 (dark) appm (a), Evolution of the temperature corresponding to $c_X = 0.5$, with $X = P$: T_m^P (dark red) and $X = O$: T_m^O (dark blue) as a function of the nominal concentration, critical temperatures of the P line (in red) and O line (in blue) are recalled (b).

Figure 5b compares the evolution of the temperatures T_m^P and T_m^O as a function of the nominal concentration with the critical temperatures T_c^P and T_c^O. If $T_m^P > T_c^P$ whatever c_{nom}, T_m^O is lower than T_c^O when c_{nom} is lower than 36 appm. When $T_m^O < T_c^O$ for a given value of c_{nom}, the concentration for the O line rich in carbon c_1 exhibits a jump due to the intra-line phase transition (see *figure 5a* for $c_{nom} = 10$ appm).

Isoconcentrations obtained from a two-equation model, that assums that all O lines have the same composition, can be compared to the current model (which does not make this assumption), by taking the average composition of the two O lines ($\langle c_O \rangle = (c_1 + c_2)/2$). The comparison is shown at $c_{nom} = 100$ appm in *figure 6*. The isoconcentration of the P line obtained with both approaches are identical (*figure 6*). The average curve of the O lines differs strongly from the curve derived from the 2-equation model. When $T \to 0$ K the average concentration is therefore ½ which is quite different from $c_O \approx 0.9$ obtained with the 2-equation model.

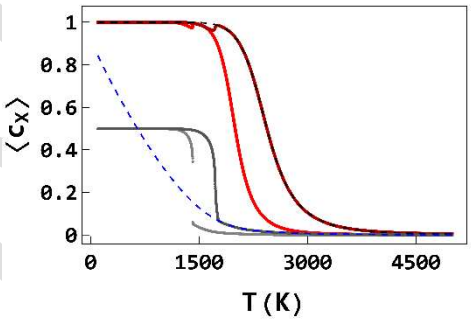

Fig. 6: Evolution of c_0 (in red), $\langle c_O \rangle = (c_1 + c_2)/2$ (in gray) concentrations with respect to the temperature for $c_{nom} = 10$ (light) and 100 (dark) appm, comparison with isoconcentrations issued from the model with only two equations for $c_{nom} = 100$ appm (dashed lines).

At low temperatures, the strong inter-O-line interaction lead to an ordered equilibrium state with one O line rich and the other poor in carbon. Hence the disordered state considered in the 2-equation model is unstable. This artificial convergence toward $c_O \approx 0.9$ when $T \to 0$ K corresponds to the cancellation of the exponential argument in the fundamental segregation equation in the disordered state:

$$-k_B T \, ln\left(\frac{c_O}{1-c_O}\right) + k_B T \, ln\left(\frac{c_{bulk}}{1-c_{bulk}}\right) = \Delta E_O^{seg,0} + 2V_{PO}c_P + V_{OO}c_O \qquad (7)$$

With $V_{OO} = 2V_{OO} + V_1 + 2V_2 + V_3 + 2V_4 = 1.37$ eV

When $T \to 0$ K the left-hand side of equation (7) tends to 0 and $c_P = 1$. So, the right-hand side of equation (7) becomes $\Delta E_O^{seg,0} + 2V_{PO} + V_{OO}c_O = 0$, which results in $c_O = 0.92$.

This result explains why, in the 2-equation model, all curves of c_O converge to 0.92 when $T \to 0$ K, whatever the nominal concentration. This is a nice artifact of the 2-equation model! The segregation enthalpy must cancel for some value of c_O, which requires an interaction term involving c_O. An interaction term means an ordered structure (or demixing) at 0 K. This shows the inadequacy of a model imposing a disordered state.

4.3 Monte Carlo results

In this section, we compare the MC isoconcentrations with the mean-field ones. The isoconcentrations are very similar (see *figure 7*). This result validates the accuracy of the 3-equation MF model. However, we can note that the MC curve of the O line rich in carbon O_1 is slightly shifted toward a lower temperature when compared with the MF curve (see *figure 7*).

In Monte Carlo, we do not expect to have a jump in temperature like in MF because the dislocation is almost a one-dimensional system. For a one-dimensional system, the critical temperature is zero, there is no phase separation. However, the alloy tendency can be characterized by the short-range order parameter defined by equation (4). A random solid solution is characterized by $\alpha_{XY} = 0$, for an ordered configuration $\alpha_{XY} < 0$, whereas $\alpha_{XY} > 0$ indicates a tendency to form homoatomic bonds with $\alpha_{XY} = 1$ for perfect two-block phase separation.

Figure 7a depicts the evolution of intra-line SRO parameter as a function of the temperature. The curves of line P and the two O lines show a positive peak characteristic of a tendency to phase separation. The peak of the prismatic line occurs around 2500 K. The value of α_{P-P} is very small because the intra-line interaction energy P is weak. For the octahedral lines the value of the SRO parameter at the peak (for T about 1600 K) is higher ($|V_{OO}| > |V_{PP}|$) showing a higher tendency to form homatomic bonds. The LRO parameter inter O-lines is equal to -1 at low temperature and to 0 at high temperature (*Figure 7b*). This the signature of a perfect ordered state which evolves toward a disordered solution when the temperature increases.

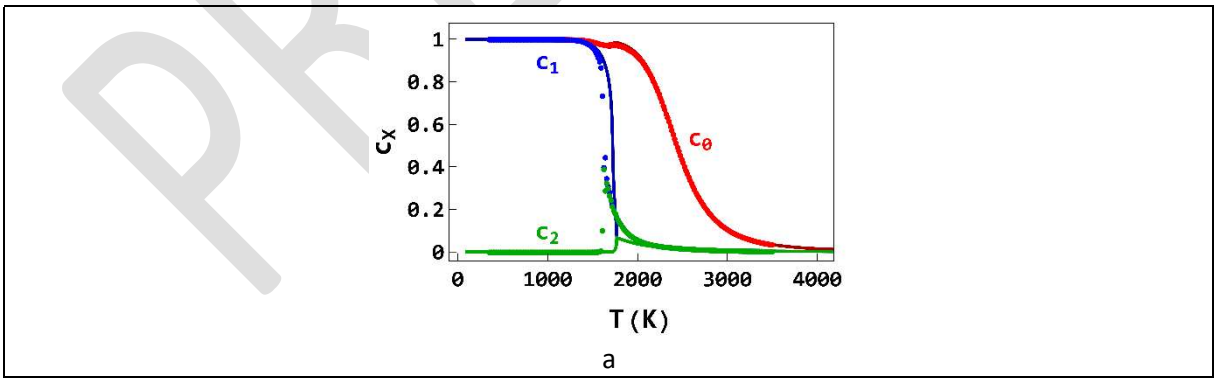

a

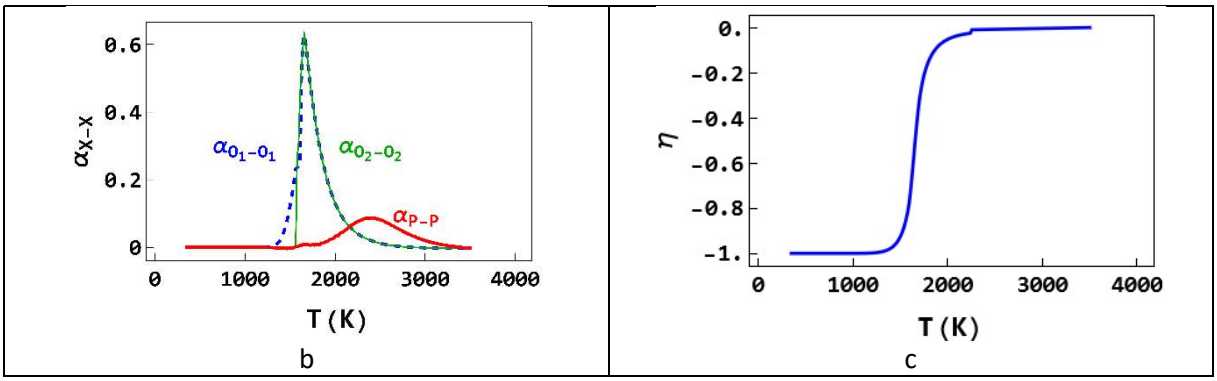

Fig. 7: Comparison between Monte Carlo (symbols) and mean field isoconcentrations (lines) for $c_{nom} = 100$ appm (a). Evolution as a function of the temperature of the Monte Carlo intra-line short range order parameter (b) and of the Monte Carlo inter-line long range order parameter η (c). (a and b) P (in red), O_1 (in blue) and O_2 (in green).

To conclude, in MC the order-disorder transition is present but the demixtion-disorder transition disappears as expected for one-dimensional systems.

4.4 Influence of the dislocation density

Isotherms and isoconcentrations can be easily obtained as a function of the nominal concentration from the previous results and from the matter conservation (Eq. 7). When the dislocation density increases the number of segregation sites increases thus the segregation can be limited to respect the matter conservation. The influence of the dislocation density is shown on the isoconcentrations for $c_{nom} = 100$ appm (*Figure 8a*) and $c_{nom} = 10$ appm (*Figure 8b*). At $c_{nom} = 100$ appm, the composition of the dislocation is identical than for the isolated dislocation whatever the temperature for $\rho = 10^{14}$ m^{-2}. For $\rho = 10^{15}$ m^{-2} the segregation is limited on the octahedral lines rich in carbon and the P-curve is slightly shifted towards the lower temperatures (*Figure 8a*). At a lower nominal concentration, $c_{nom} = 10$ appm, the isoconcentrations are unchanged at $\rho = 10^{13}$ m^{-2}. At higher dislocation density the segregation is limited (*Figure 8b*). For $\rho = 10^{14}$ m^{-2} the same profile as above (for $c_{nom} = 100$ appm and $\rho = 10^{15}$ m^{-2} see *Figure 8a*) is observed. As the dislocation density increases, for $\rho = 10^{15}$ m^{-2}, the concentration of all octahedral lines is zero at any temperature and the concentration of prismatic sites is limited to about 0.2 at low temperatures (*Figure 8b*).

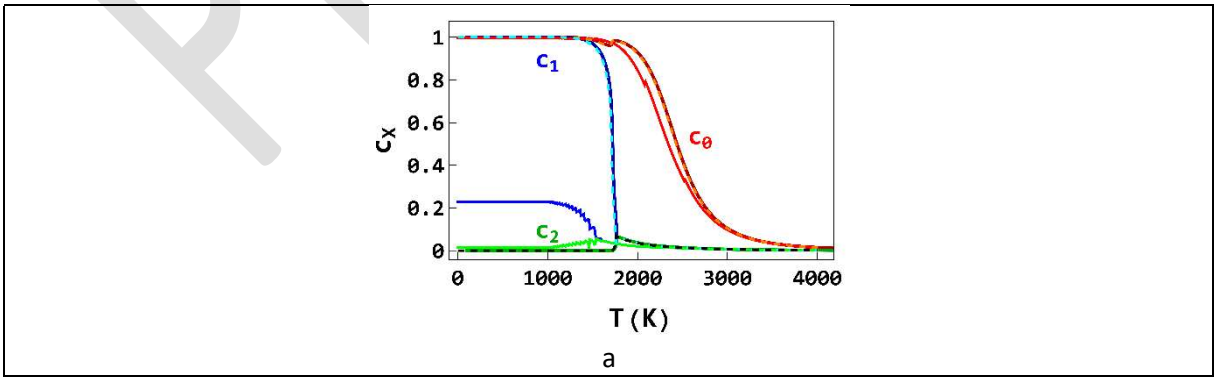

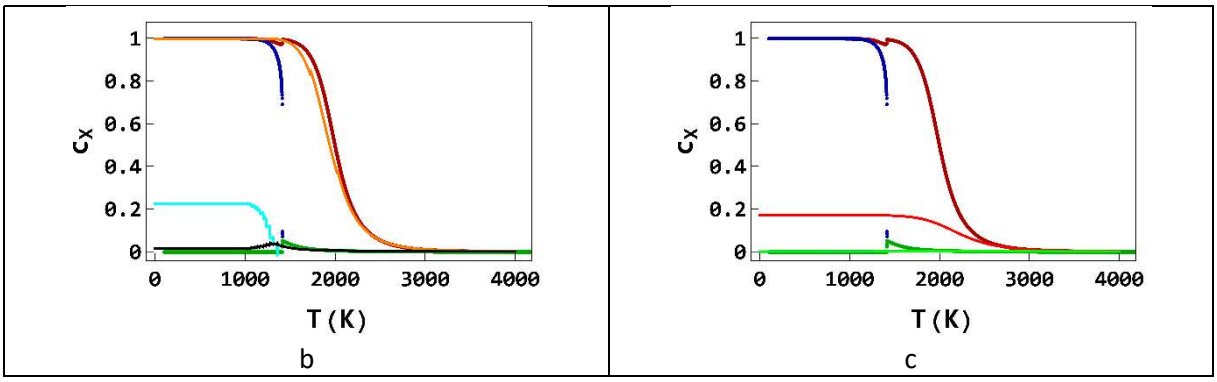

Fig. 8: Influence of the dislocation density on the isoconcentrations for $c_{nom} = 100$ appm (a), $c_{nom} = 10$ appm (b and c) (c). (a) single dislocation (thick dark lines : red for P, blue for O_1 and green for O_2), $\rho = 10^{14}$ (dashed lines : orange for P, cyan for O_1 and black for O_2) and $\rho = 10^{15}$ (thin lines: red for P, blue for O_1 and green for O_2) ; (b) single dislocation (thick dark dots : red for P, blue for O_1 and green for O_2), $\rho = 10^{14}$ (orange for P, cyan for O_1 and gray for O_2) ; (c) single dislocation (thick dark dots : red for P, blue for O_1 and green for O_2), $\rho = 10^{15}$ (thin lines : red for P, blue for O_1 and green for O_2) (c). For $c_{nom} = 10$ appm, profiles are identical for $\rho = 10^{14}$ and $\rho = 10^{13}$ (not drawn).

The influence of dislocation density on the isoconcentrations can be easily dealt in the disordered state by considering equation (7) and the isoconcentrations of the dislocation alone. From the profile we assume that $c_2 = 0$ for three octahedral lines and that c_{bulk} is negligible. Thus, Eq. 7 can be rewritten as $c_{nom} = 3\rho\frac{a^3}{6b}(c_0 + 3c_1)$. From this relationship we calculate

- the value of ρ from which the segregation is limited by the dislocation density. For $c_0 = c_1 = 1$ the right-hand side term is about $10^{-19}\rho$. By writing $c_{nom} = 10^{-n}$, the dislocation density starts to restrict segregation for $\rho > 10^{19-}$, *i.e.* 10^{15} m^{-2} for $c_{nom} = 10^{-4}$ (100 appm) and $\rho > 10^{14}$ m^{-2} for $c_{nom} = 10^{-5}$ (10 appm).
- the value of c_1 when the segregation is limited on the O_1-line. c_1 is given by $c_1 = \left(\frac{2\,b}{\rho a^3}\,c_{nom} - c_0\right)/3$ with $c_0 = 1$, resulting in $c_1 = 0.24$. This result is very different from the one obtained with a two-equation model.
- the value of c_0 when the segregation is limited on the P-line. All O-lines are empty and $c_0 = \frac{2\,b}{\rho a^3}\,c_{nom} = 0.17$.

All these results are in perfect agreement with the full calculation.

5. Discussion

In this paper, we have investigated the segregation of carbon atoms in screw dislocations of tungsten using a mean-field model and Monte Carlo simulations. The mean field model describes the behavior of the prismatic line and two octahedral lines to observe a hypothetical ordered state. This MF model predicts an intra P-line transition at low temperatures for negligible bulk concentrations, so experimental evidence should not be possible. At low temperatures the sites of the prismatic line are occupied by carbon atoms. From about 2200 K the carbon concentration of the prismatic line decreases with increasing temperature (for $c_{nom} = 100$ appm). The behavior of the octahedral lines is more complex. We find, at low temperatures, that one octahedral line is saturated in carbon atoms and the other without any, forming an alternative sequence. The concentration of carbon of the rich O-line decreases from 1700 K (for $c_{nom} = 100$ appm). In addition, at temperatures up to 1600 K, an intra-line demixing/disordering transition occurs. This transition is characterized by a concentration jump on the isoconcentration curves when the nominal concentration is below 36 appm.

Our mean field results are very different from those obtained with a model that assumes that all O-lines have the same behavior. The temperatures for which the P-line is predicted to be saturated with carbon and all O-lines are empty are between 1800K and 2300K. At lower temperatures three O-lines are rich in carbon.

In Monte Carlo, we also find the inter O-line order/disorder transition while the intra line demixtion/disorder transitions disappear as the lines are almost one dimensional. The evolution of the carbon concentration on the different segregation sites with respect to temperature shows the order state at low temperatures with every second line carbon saturated (*Figure 9a*). When the temperature increases, during the concentration decrease of the carbon-rich line O_1 and the O_2 is still nill, the local intra O_1-line order parameter increases and the inter-line order parameter decreases (in absolute value) (*Figure 9b*): clusters of empty sites appear in rich O_1 lines. In the second part of the O_1 concentration decrease, O_1 and O_2 lines have almost the same composition. The octahedral lines O_1 and O_2 are composed of carbon clusters and clusters of empty sites (*Figure 9c*). Lines O_1 and O_2 have thus the same SRO intra-line parameter. The inter O-line order parameter decreases (in absolute value) and it is still negative because carbon clusters on a O-line are in first neighboring of empty clusters on another O-line.

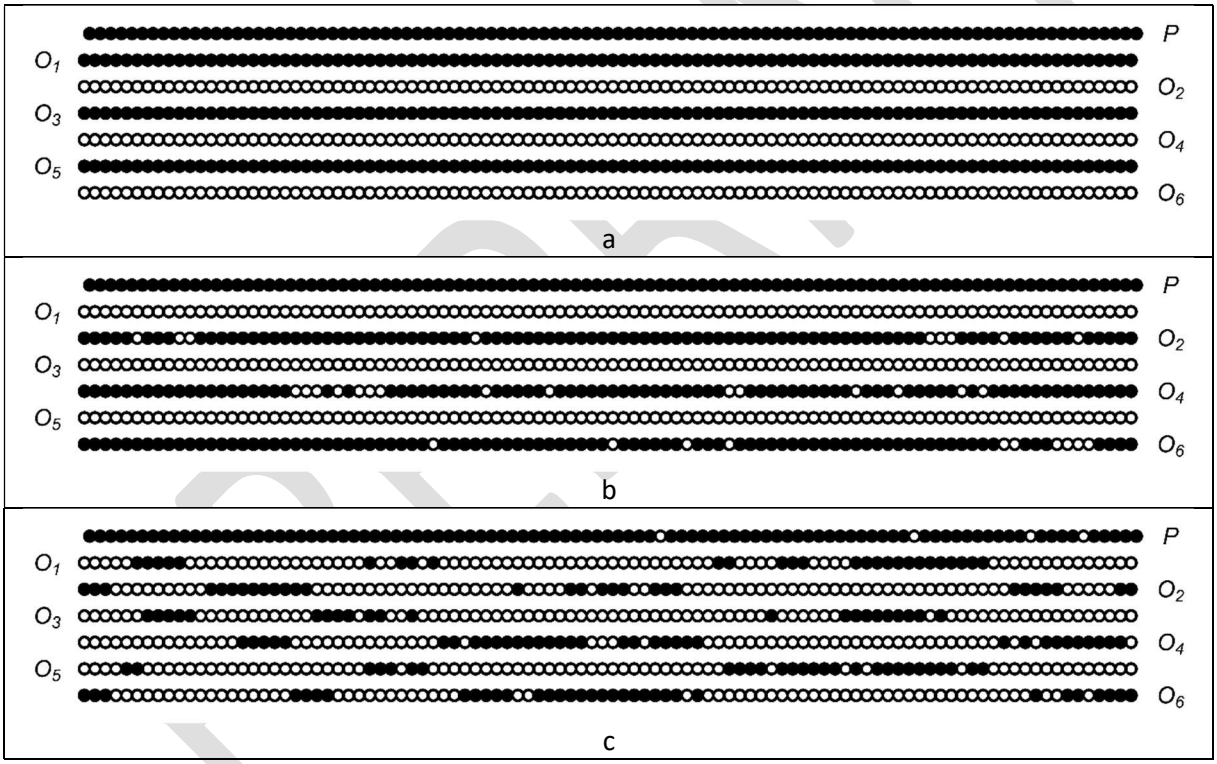

Fig. 9: Monte Carlo microstructures obtained for a single dislocation for $c_{nom} = 100$ appm at $T = 1280\ K$ (a), $T = 1595\ K$ (b), $T = 1673\ K$ (c).

Segregation on dislocations leads to a large variety of phenomena, which cannot be described systematically by oversimplified models. The choice of the model depends on the complexity of the system. The comparison with MC simulations allows to validate the relevance of the chosen model. Our results illustrate the complexity when two phase transitions intertwine.

Acknowledgements

We thank L. Ventelon for giving us the opportunity to study the segregation on dislocations.

References

[1] G. Hachet, L. Ventelon, F. Willaime, and E. Clouet, *Screw Dislocation-Carbon Interaction in BCC Tungsten: An Ab Initio Study*, Acta Mater. **200**, 481 (2020).

[2] G. Hachet, D. Caillard, L. Ventelon, and E. Clouet, *Mobility of Screw Dislocation in BCC Tungsten at High Temperature in Presence of Carbon*, Acta Mater. **222**, 117440 (2022).

[3] Y. Kuk, P. J. Silverman, and T. M. Buck, *Structure of Segregated Au Layers on Ni(110) – 0.8 at. % Au Alloy by Scanning Tunneling Microscopy*, Phys. Rev. B **36**, 3104 (1987).

[4] S. H. and V. P. . Schmidt M, *Direct Observation of Local Chemical Surface Properties by Scanning Tunneling Microscopy*, Phys. Rev. Lett. **70**, 1441 (1993).

[5] K. L. Merkle, *High-Resolution Electron Microscopy of Interfaces in Fcc Materials*, Ultramicroscopy **37**, 130 (1991).

[6] T. T. Tsong, *Atom-Probe Field Ion Microscopy and Applications to Surface Science*, Surf. Sci. **299**–**300**, 153 (1994).

[7] D. Blavette, A. Bostel, J. M. Sarrau, B. Deconihout, and A. Menand, *An Atom Probe for Three-Dimensional Tomography*, Nature **363**, 432 (1993).

[8] M. K. Miller, *Atom Probe Tomography Characterization of Solute Segregation to Dislocations and Interfaces*, J. Mater. Sci. **41**, 7808 (2006).

[9] S. Piazolo, A. La Fontaine, P. Trimby, S. Harley, L. Yang, R. Armstrong, and J. M. Cairney, *Deformation-Induced Trace Element Redistribution in Zircon Revealed Using Atom Probe Tomography*, Nat. Commun. **7**, 10490 (2016).

[10] G. Tréglia, B. Legrand, and F. Ducastelle, *Segregation and Ordering at Surfaces of Transition Metal Alloys: The Tight-Binding Ising Model*, Europhys. Lett. **7**, 575 (1988).

[11] I. Meunier, G. Tréglia, R. Tétot, J. Creuze, F. Berthier, and B. Legrand, *Misfit Dislocation Loops or Incommensurate Structure at an Interface: Vibrational and Anharmonic Effects*, Phys. Rev. B **66**, 125409 (2002).

[12] R. Tétot, F. Berthier, J. Creuze, I. Meunier, G. Tréglia, and B. Legrand, *Cu-Ag (111) Polymorphism Induced by Segregation and Advacancies*, Phys. Rev. Lett. **91**, 1 (2003).

[13] J. Creuze, F. Berthier, R. Tétot, and B. Legrand, *Phase Transition Induced by Superficial Segregation: The Respective Role of the Size Mismatch and of the Chemistry*, Surf. Sci. **491**, 1 (2001).

[14] D. N. Seidman, B. W. Krakauer, and D. Udler, *Atomic Scale Studies of Solute-Atom Segregation at Grain Boundaries: Experiments and Simulations*, J. Phys. Chem. Solids **55**, 1035 (1994).

[15] J. D. Rittner and D. N. Seidman, *Solute-Atom Segregation to 〈110〉 Symmetric Tilt Grain Boundaries*, Acta Mater. **45**, 3191 (1997).

[16] F. Berthier, B. Legrand, and G. Tréglia, *How to Compare Superficial and Intergranular Segregation? A New Analysis within the Mixed SMA–TBIM Approach*, Acta Mater. **47**, 2705 (1999).

[17] J. Creuze, F. Berthier, R. Tétot, and B. Legrand, *Wetting and Structural Transition Induced by Segregation at Grain Boundaries: A Monte Carlo Study*, Phys. Rev. Lett. **86**, 5735 (2001).

[18] B. Lüthi, F. Berthier, L. Ventelon, B. Legrand, D. Rodney, and F. Willaime, *Ab Initio Thermodynamics of Carbon Segregation on Dislocation Cores in Bcc Iron*, Model. Simul. Mater.

Sci. Eng. **27**, 074002 (2019).

[19] I. Medouni, A. Portavoce, P. Maugis, P. Eyméoud, M. Yescas, and K. Hoummada, *Role of Dislocation Elastic Field on Impurity Segregation in Fe-Based Alloys*, Sci. Rep. **11**, 1780 (2021).

[20] G. Rossi, R. Ferrando, and C. Mottet, *Structure and Chemical Ordering in CoPt Nanoalloys*, Faraday Discuss. **138**, 193 (2008).

[21] D. Cheng, S. Yuan, and R. Ferrando, *Structure, Chemical Ordering and Thermal Stability of Pt-Ni Alloy Nanoclusters*, J. Phys. Condens. Matter **25**, (2013).

[22] F. Lequien, J. Creuze, F. Berthier, and B. Legrand, *Superficial Segregation in Nanoparticles: From Facets to Infinite Surfaces*, J. Chem. Phys. **125**, 094707 (2006).

[23] F. Lequien, J. Creuze, F. Berthier, I. Braems, and B. Legrand, *Superficial Segregation, Wetting, and Dynamical Equilibrium in Bimetallic Clusters: A Monte Carlo Study*, Phys. Rev. B **78**, 075414 (2008).

[24] V. Moreno, J. Creuze, F. Berthier, C. Mottet, G. Tréglia, and B. Legrand, *Site Segregation in Size-Mismatched Nanoalloys: Application to Cu–Ag*, Surf. Sci. **600**, 5011 (2006).

[25] E. Maras, F. Berthier, and B. Legrand, *Stability Diagram of Janus and Core–Shell Configurations in Bimetallic Nanowires*, J. Phys. Chem. C **120**, 22670 (2016).

[26] N. Metropolis, A. W. Rosenbluth, M. N. Rosenbluth, A. H. Teller, and E. Teller, *Equation of State Calculations by Fast Computing Machines*, J. Chem. Phys. **21**, 1087 (1953).

[27] J. Goldschmidt and J. A. Brand, *The Tungsten-Rich*, **5**, 181 (1963).